Magnetic and superconducting properties of holmium-rich $(Er_{1-x}Ho_x)Rh_4B_4$

J. W. Lynn and J. A. Gotaas
Department of Physics, University of Maryland, College Park, Maryland 20742
and Center for Materials Research, National Bureau of Standards, Gaithersburg, Maryland 20899

R. N. Shelton
*Ames Laboratory—U.S. Department of Energy and Department of Physics, Iowa State University, Ames, Iowa 50011**
and Département de Physique de la Matière Condensée, Université de Genève, CH-1211 Genève 4, Switzerland

H. E. Horng†
Ames Laboratory—U.S. Department of Energy and Department of Physics, Iowa State University, Ames, Iowa 50011

C. J. Glinka
Center for Materials Research, National Bureau of Standards, Gaithersburg, Maryland 20899
(Received 19 November 1984)

Neutron scattering, susceptibility, and resistivity measurements have been carried out on $(Er_{1-x}Ho_x)Rh_4B_4$ for concentrations $x=1.0$, 0.89, 0.84, and 0.75, which span the "multicritical" point ($x_c \approx 0.9$) where the magnetic and superconducting phase boundaries meet. For all concentrations studied a transition to long-range ferromagnetic order is observed, with the Ho moments ordering along the tetragonal axis. The spins are in fact locked along the c axis by strong crystal-field anisotropies, yielding Ising-like magnetic behavior in this concentration region. The temperature dependence of the order parameter is mean-field-like, suggesting that the range of the magnetic interactions is large, and we attribute this behavior to the importance of dipolar interactions. In the concentration range $x < x_c$ where superconductivity is observed, the magnetic transition appears to be continuous and reversible, and occurs within the nominal superconducting interval $T_{c2}(x) < T < T_{c1}(x)$. Thus there is some kind of "coexistence" of long-range magnetic order and superconductivity in the samples, but the nature of this coexistence cannot be determined unambiguously. In particular the experimental evidence in this system is not sufficient to decide if there is true microscopic coexistence, or whether some portions of the sample are ferromagnetic and normal while other regions are superconducting and paramagnetic (or magnetically ordered with a very-long-wavelength sinusoidal periodicity). Below T_M strongly-temperature-dependent small-angle scattering is observed, characterized by a cross section of the Porod form $S(Q)=A(T)/Q^4$, where $A(T)$ increases monotonically with decreasing temperature. This wave-vector dependence is consistent with the assumption that the scattering originates from domain walls whose widths are large compared to the inverse-Q range explored ($\lesssim 300$ Å). In particular, no oscillatory component to the magnetization was observed for any concentration or temperature within the experimentally accessible wave-vector range of $Q > 0.003$ Å^{-1}, in contrast to the behavior of $ErRh_4B_4$. At the lowest concentration studied (75 at. % Ho) the magnetization was found to be reduced in the temperature region where superconductivity appeared. The magnetic order parameter, however, was still found to be continuous and reversible.

I. INTRODUCTION

The interplay between superconductivity and magnetism has received considerable attention in recent years since the discovery of ternary rare-earth superconducting compounds which order magnetically.[1] For the case of ferromagnetic ordering there is strong competition between the magnetic and superconducting order parameters, which leads to rich and interesting behavior. In the compounds studied in detail so far, $ErRh_4B_4$,[2,3] $HoMo_6S_8$,[4,5] and $HoMo_6Se_8$,[6] superconductivity sets in at T_{c1} and then they order magnetically at much lower temperatures ($T_M \ll T_{c1}$). The competition between the superconductivity and ferromagnetism initially results in a long-wavelength ($\sim 10^2$ Å) oscillatory component to the magnetization developing in the superconducting state. For $ErRh_4B_4$ and $HoMo_6S_8$ this oscillatory magnetic phase exists only in a limited temperature interval, with the superconductivity being destroyed (at T_{c2}) and pure ferromagnetism setting in at sufficiently low temperatures.[3,5,7–10] For $HoMo_6Se_8$, on the other hand, this coexistence state may be indicative of the ground-state properties.[6]

In the (Er-Ho)Rh_4B_4 alloy series of interest here, pure $ErRh_4B_4$ becomes superconducting at 8.6 K, and then reenters the normal conducting phase at 0.7 K as ferromagnetism sets in.[2,3,7,8] In the intervening temperature range, below ~ 1.2 K, both ferromagnetism and a

sinusoidal component to the magnetization coexist with superconductivity. The amplitude of any critical fluctuations is very small in this material, and both the ferromagnetic and sinumagnetic order parameters appear to be "smeared," with no clear indication of where the magnetic phase transition T_M is located. One possible interpretation which was advanced to explain this behavior was that the smearing originated from inhomogeneities in the polycrystalline specimens,[3,7] but essentially identical results have been obtained on a single-crystal sample more recently,[8] and the precise nature of the magnetic-superconducting state in this material is still not completely understood. One important experimental point which has emerged is that the Er magnetic moments are constrained by crystal-field anisotropies to lie in the (tetragonal) basal plane, rendering both the magnetic and superconducting properties highly anisotropic.[11,12]

With the substitution of holmium for erbium, all three phase boundaries (T_{c1}, T_{c2}, T_M) initially decrease slowly in temperature with increasing holmium concentration. Near $x \sim 0.25$, T_{c2} and T_M reverse direction and increase with increasing x, and the boundaries meet at a "multicritical" point for $x_c \sim 0.9$ and a temperature of about 6 K as shown in Fig. 1.[13,14] The crystal-field anisotropies

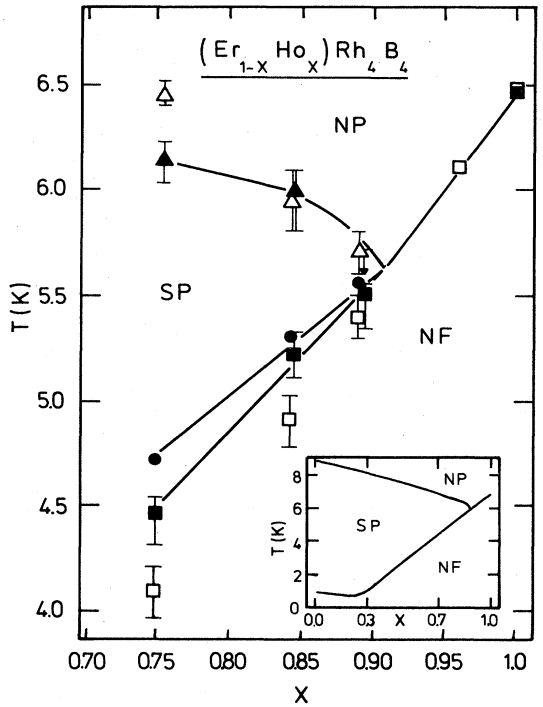

FIG. 1. Low-temperature phase diagram for the system $(Er_{1-x}Ho_x)Rh_4B_4$ near the critical concentration ($x \approx 0.9$) determined by ac susceptibility measurements (△□,▲■) and neutron scattering (●). Filled symbols represent data obtained from measurements on samples in the powdered form, while open symbols are data taken on ingots. For the $x = 0.89$ sample, the transition into the superconducting state is incomplete before the onset of ferromagnetism. The inset is taken from Ref. 13 to illustrate the phase diagram for all values of x. Three distinct regions are labeled: normal paramagnetic (NP), superconducting paramagnetic (SP), and normal ferromagnetic (NF).

favor the Ho moments pointing along the c axis,[11,15–19] and in fact the anisotropy is sufficiently strong to render the system Ising-like in the holmium-rich regime as we shall see below. Hence, the coupling between the Er and Ho moments in the alloy is very small, and the two types of ions order essentially independently. The behavior of the magnetic-phase boundary therefore is dominated by the holmium moments ordering first with decreasing temperature for $x > \sim 0.25$, while the Er moments order first for $x < \sim 0.25$.

We have been carrying out a systematic study of the magnetic and superconducting properties in the holmium-rich region in an effort to determine the nature of the competition between magnetic order and superconductivity in the regime where these two competing energies are approximately equal. Our original intention was to observe the change in the sinusoidal magnetization near x_c as a function of concentration, or equivalently as a function of pressure,[20] but we have not been able to obtain any evidence for an oscillatory magnetic structure in this concentration regime. Indeed, the magnetic order always appears to be ferromagnetic in nature within our experimental resolution, with a temperature interval of coexistence.[15,16] It is not possible, however, to establish whether this coexistence is microscopic in nature, i.e., whether the same regions in the crystal are both magnetically ordered and superconducting simultaneously, or whether some regions are superconducting and paramagnetic (or a very-long-wavelength sinusoidal magnetism), while other regions are ferromagnetic and normal. At intermediate x we find a clear suppression of the magnetic order parameter when superconductivity is present, in agreement with the behavior observed[17] at lower concentrations ($x = 0.6$), but we find no hysteresis in the magnetization.

In Sec. II we discuss the sample preparation and the experimental techniques we have used to obtain the resistivity, susceptibility, crystal-field excitations, and the wave-vector-dependent magnetization. In Sec. III we first discuss the behavior of the end compound $HoRh_4B_4$, which is not superconducting. Crystal-field anisotropies render this compound a good approximation to a three-dimensional Ising system, with mean-field behavior. In particular we present our neutron-diffraction results as a function of temperature and applied magnetic field; a detailed analysis of the crystal-field effects will be given elsewhere.[11] We will then present our results for $x \lesssim x_c$, paying particular attention to the temperature interval where magnetic order develops. We will compare the present results with the behavior observed in related systems such as $HoMo_6S_8$ and $HoMo_6Se_8$, and discuss how our results address the question of the "coexistence of ferromagnetism and superconductivity" in the context of various theoretical models that have been advanced. In Sec. IV we summarize our results and conclusions, and discuss possible directions for new experiments.

II. EXPERIMENTAL PROCEDURES

A. Sample preparation and bulk magnetic measurements

All samples used in this study were prepared using the highest-purity, Ames Laboratory rare-earth metals (≤ 15

ppm of any metallic impurity) together with commercially supplied rhodium (99.9%, Thiokol Corp., Alfa Products) and ^{11}B isotope obtained from Eagle-Pitcher. The isotope of boron was used to avoid the very high neutron-absorption cross section of natural boron. For each sample, stoichiometric amounts of the necessary elements were melted together in a Zr-gettered argon arc furnace. The resulting ingot was turned and remelted at least six times to promote homogeneity. Mass loss was always less than 0.1%. Each sample was then sealed in a Ta tube, which was in turn sealed in a quartz ampoule and annealed for one week at 1200 °C followed immediately by one week at 800 °C. No impurity phases were detected by slow-scan powder x-ray diffraction data, indicating that any impurity-phase content was below the readily detectable limit of 5%.

Neutron diffraction did reveal the presence of some impurity phases, one of which was magnetic ($T_M \sim 19$ K), but the volume of these phases was $\sim 1\%$ or less. Susceptibility, resistivity, and neutron-scattering measurements were all carried out on identical samples to facilitate comparison of results. Low-frequency (~ 17 Hz) ac inductance measurements were performed on samples in both the ingot and powdered form to determine the critical temperatures. A standard ^4He cryostat was used for experiments above 1.1 K, while a commercial (S. H. E. Corp.) ^3He-^4He dilution refrigerator was employed for susceptibility experiments down to 20 mK. Electrical resistivity measurements were done via a four-lead, low-frequency ac method. Platinum leads (0.002 in. diameter) were spot welded onto regularly shaped samples with a rectangular cross section. The thermometry consisted of germanium resistance thermometers for temperatures below 30 K and platinum resistance thermometers at higher temperatures.

B. Neutron-scattering measurements

Even though the ^{11}B isotope was used in preparing the samples, the materials were still quite absorbing for neutrons due to the high-absorption cross section of Rh, which has only one stable isotope. All the neutron measurements were therefore carried out on powders which were mounted between thin aluminum plates to utilize flat-plate geometry. The sample holder was then mounted in an aluminum sample chamber filled with an atmosphere (STP) of helium to facilitate thermal conduction between the sample and the cold finger upon which the sample chamber was mounted. A calibrated Ge resistor was used to measure the temperature, and in particular to determine the magnetic transition temperatures in zero field.

For the field-dependent work the samples were mounted in a flow Dewar, which could then be inserted in a split-coil superconducting magnet. The magnetic field at the sample position was perpendicular to the horizontal, with an adjustable magnitude up to 7 T. The sample temperature in this case was monitored by a GaAs diode sensor.

The diffraction and inelastic scattering measurements were taken with standard triple-axis neutron spectrometers located at the National Bureau of Standards Research Reactor. Pyrolytic graphite monochromators, analyzers, and higher-order filters were employed at a neutron energy of 14 meV. The angular collimations before and after the monochromator and analyzer were varied between 10 and 40 min depending on the intensity and resolution requirements of the measurements.

The crystal structure of the ternary rhodium borides is tetragonal with space group $P4_2/nmc$, which contains two formula units of RRh_4B_4 per unit cell[21] (R = rare earth). The rare-earth positions are fixed by symmetry in the unit cell to (0, 0, $\frac{1}{2}$) and ($\frac{1}{2}$, $\frac{1}{2}$, 0), whereas the Rh and B positions have to be determined by detailed crystallographic analysis. Once the chemical structure is known, the nuclear Bragg cross sections can be calculated and then can serve to put the magnetic peaks on an absolute basis.

For our particular case of flat-plate geometry the integrated intensity from a nuclear-powder diffraction peak is given by[22]

$$I_N = C\frac{|F_N(hkl)|^2 m_{hkl} t e^{-\mu t \sec\theta} e^{-2W}}{\sin^2(2\theta)}, \tag{1}$$

where (hkl) are Miller's indices for the reciprocal-lattice vector τ, t is the thickness of the sample, μ is the linear absorption coefficient, 2θ is the scattering angle, and m_{hkl} is the multiplicity of the reflection. The coefficient C is a constant that contains the details of the instrument, and F_N is the nuclear-structure factor for the reflection of interest:

$$\left[\frac{d\sigma}{d\Omega}\right]_{\text{nuclear}} = |F_N|^2 = \left|\sum_{j=1}^{N'} c_j b_j e^{i\tau\cdot r_j}\right|^2, \tag{2}$$

where b_j is the coherent nuclear-scattering length, c_j is the occupancy of the jth atom located at $\mathbf{r}_j$, and the sum extends over all atoms N' in the unit cell. For the $\mathbf{r}_j$ of Rh and B we used the coordinates determined by Vandenberg and Matthias[21] as modified by Moncton *et al.*,[3] along with the coherent scattering amplitudes $b_{Ho}=0.85$, $b_{Er}=0.80$, $b_{Rh}=0.584$, and $b_{^{11}B}=0.61$ (all in units of 10^{-12} cm).

For magnetic Bragg scattering we have a similar type of expression for the integrated intensity:

$$I_M = C\left[\frac{\gamma e^2}{2mc^2}\right]^2 \langle\mu^z(T,H)\rangle^2 f^2(\tau)\langle 1-(\hat{\tau}\cdot\hat{\mathbf{M}})^2\rangle \times \frac{m_{hkl} t e^{-\mu t\sec\theta} e^{-2W} |F_M(hkl)|^2}{\sin^2(2\theta)}, \tag{3}$$

where

$$\frac{\gamma e^2}{2mc^2} = -0.2695\times 10^{-12} \text{ cm}$$

is the neutron-electron dipole coupling constant, $\langle\mu^z\rangle$ is the thermal average of the z component of the magnetic moment at each rare-earth site, $f(\tau)$ is the value of the magnetic form factor (Fourier transform of the atomic

magnetization density), and $\hat{\tau}$ and $\hat{\mathbf{M}}$ are unit vectors in the direction of τ and the magnetization, respectively. Finally, F_M is the magnetic-structure factor analogous to Eq. (2) but with b_j replaced by unity and the sum in the unit cell taken over magnetic ions only. In the present simple case $F_M=2$ or 0. The angular brackets $\langle\ \rangle$ denote an average over equivalent reciprocal-lattice vectors and domain possibilities. In a ferromagnet we can obtain a simplified comparison by choosing reflections at the same angular setting. Then

$$\frac{I_M}{I_N}=4\left[\frac{\gamma e^2}{2mc^2}\right]^2\frac{\langle\mu^z\rangle^2 f^2(\tau)\langle 1-(\hat{\tau}\cdot\hat{\mathbf{M}})^2\rangle}{|F_N|^2}\ , \tag{4}$$

from which we obtain the desired quantity

$$\langle\mu^z(H,T)\rangle=\frac{1.855\,|F_N|}{|f(\tau)|}\left[\frac{1}{\langle 1-(\hat{\tau}\cdot\hat{\mathbf{M}})^2\rangle}\frac{I_M}{I_N}\right]^{1/2}, \tag{5}$$

where $\langle\mu^z\rangle$ is in Bohr magnetons μ_B. The relative field and temperature dependence of the magnetization can be directly determined from the measurements, and these data can in turn be put on an absolute basis with the aid of the nuclear-scattering intensities.

For the measurements at small wave vectors Q we utilized the small-angle scattering facility at the National Bureau of Standards (NBS).[23] This instrument employs a helical velocity selector to determine the desired neutron-wavelength incident on the sample, usually between 4 and 10 Å. The angular distribution of scattered neutrons is measured with a two-dimensional position-sensitive detector placed in the vicinity of the forward-beam direction. In the present case of interest, where the sample is polycrystalline and no magnetic field is applied, the scattering must be symmetrically distributed about $\mathbf{Q}=0$. We thus obtain the intensity of scattered neutrons as a function of the magnitude of the wave vector $\mathbf{Q}$. It should be kept in mind that in this experimental configuration we cannot obtain information about any possible anisotropic distribution of scattering in the sample, which information can be obtained only with single-crystal specimens.

III. RESULTS

A. $HoRh_4B_4$

This compound becomes ferromagnetic at 6.5 K but is not superconducting at any temperature as indicated in Fig. 1. The magnetic properties themselves are nevertheless quite interesting and we summarize the findings of a number of studies[13–20,24] before presenting our field- and temperature-dependent diffraction data.

A preliminary study[19] showed that the tetragonal c axis is the preferred magnetic direction in the ordered state, with an (extrapolated) low-temperature moment of $8.7\mu_B$. Subsequent magnetization and specific-heat measurements[14,17,18] showed that the magnetic properties could be very well described by an $S=\frac{1}{2}$ Ising-like mean-field model. A detailed crystal-field analysis[11] using magnetization, specific heat, Mössbauer and inelastic neutron-scattering measurements confirmed that the crystal-field ground state is a doublet, with the first excited state at an energy corresponding to 50 K. Thus, to a good approximation only the doublet is involved in the magnetic phase transition.

Our magnetic diffraction pattern for $HoRh_4B_4$ is shown in Fig. 2. Measurements were taken both above (7.00 K) and below (1.35 K) the magnetic ordering temperature, and the two data sets were subtracted point by point. In such a subtraction the nuclear Bragg peaks and incoherent nuclear scattering cancel (in the absence of any nuclear spin ordering), along with room background, leaving only changes in the inelastic magnetic scattering and magnetic Bragg peaks. The most evident features are the intense magnetic Bragg reflections such as the {101} and {110}, whose widths are resolution limited indicating that long-range ferromagnetic order has been established. In addition we find no magnetic contribution to the {002} peak, which shows via Eq. (2) that $\hat{\tau}\cdot\hat{\mathbf{M}}=1$ for this reflection. Hence the Ho^{3+} moments must point along the c axis. These conclusions are readily evident directly from the observed data and are in good agreement with previous work.[17,19] One noteworthy point of Fig. 1 is that the subtracted intensities are negative in between the Bragg peaks, revealing that there is a reduction in the scattering when the moments order. This is a necessary consequence of the sum rules on the magnetic scattering; above T_M all the magnetic scattering is inelastic and diffuse, while in the fully ordered state most of the magnetic intensity resides in the (purely elastic) Bragg peaks.

To put the magnetic intensities on an absolute basis we calculated the nuclear cross sections as discussed in Sec. II B. For the {101} reflection, for example, we find $|F_N|^2=0.2695$ b. The measured integrated intensities above T_M and at low temperatures then yield from Eq. (5) a c-axis magnetic moment of

$$\mu^c(T=0)=(8.58\pm 0.34)\mu_B\ .$$

We have used the calculated[25] spherical component $\langle j_0\rangle=0.95$ for the magnetic form factor for this evaluation since the aspherical component is small for these

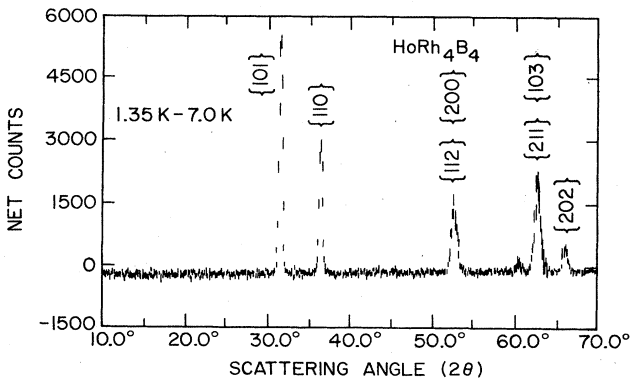

FIG. 2. Magnetic diffraction pattern for $HoRh_4B_4$ taken with a triple-axis spectrometer set for elastic scattering and an incident neutron wavelength of 2.3509 Å. The magnetic contribution is obtained by subtracting the data measured at 7.0 K from the data at 1.35 K.

low-angle peaks and the measurements are on a powder. Our value is in good agreement with the value of $(8.7\pm0.3)\mu_B$ reported by Lander *et al.*[19] A similar analysis for the {002} Bragg peak reveals that any ordered moment perpendicular to the c axis must be less than $0.4\mu_B$.

The quoted error of $0.34\mu_B$ in the determination of the absolute value of the moment is due only to statistical accuracies associated with the {101} magnetic and nuclear intensities, and in particular does not include any allowance for uncertainties in the calculations of $|F_N|$. In the present case, these systematic uncertainties may be substantial since the calculated $|F_N|$ are small in magnitude for the low-angle peaks due to the compensation of the terms in Eq. (2). To check the accuracy of $|F_N|$ we therefore carried out a low-temperature (18 K) profile refinement for the $HoRh_4B_4$ sample. We obtained $x_{Rh}=0.247(1)$, $z_{Rh}=0.145(1)$, $x_B=0.330(1)$, and $z_B=0.851(1)$, which are close to the values obtained for $ErRh_4B_4$; the new values yielded $|F_N|^2=0.2584$ b with a resultant moment of $8.40\mu_B$. We also tried refining the occupancies of the Ho, Rh, and B sites to determine the sensitivity of $|F_N|$ to them, and obtained the same result within experimental error. We remark that this latter procedure also checks for possible discrepancies in the values of the nuclear-scattering amplitudes, which can also change $|F_N|$. Based on this analysis we may estimate a possible additional error of $0.5\mu_B$ in the absolute magnitude of μ. The crystal-field model[11] predicts a ground-state moment of $10\mu_B$, which appears to be outside our combined experimental errors. Bulk magnetization measurements also indicate[11] a reduced moment.

The intensity of the {101} Bragg peak is shown in Fig. 3 as a function of temperature. The phase transition to the ferromagnetic state occurs at 6.47 K. Note that there is very little critical scattering associated with the phase transition, a point to which we will return when we discuss the small-angle measurements. In addition, the magnetic intensity is very close to linear in the vicinity of T_M. For a three-dimensional ferromagnet we generally would expect the magnetization to follow a power-law behavior sufficiently close to the transition, with a critical exponent β:

$$M=M_0\left[\frac{T_c-T}{T_c}\right]^{\beta}. \tag{6}$$

Since the intensity is proportional to the square of the magnetization as indicated in Eq. (3), we would expect the magnetic intensity near T_c to obey a relationship of the form

$$I=I_0 t^{2\beta}, \tag{7}$$

where $t=1-T/T_c$ is the reduced temperature. The observed linearity of the intensity then implies $\beta=\frac{1}{2}$, the mean-field result. All the magnetic properties for this material are in fact well represented by mean-field theory,[14,18] and the solid curve in the figure is just the mean-field result for $S=\frac{1}{2}$. A detailed comparison of such a model with the experimental observations has already been carried out by Ott *et al.*[18] We remark that, from a pragmatic standpoint, the weak critical scattering and the linear intensity with temperature make it relatively straightforward to determine the magnetic ordering temperatures for these holmium-rich materials, and this is an important attribute when comparing the magnetic and superconducting measurements for $x<1$.

Above the magnetic phase transition there is of course

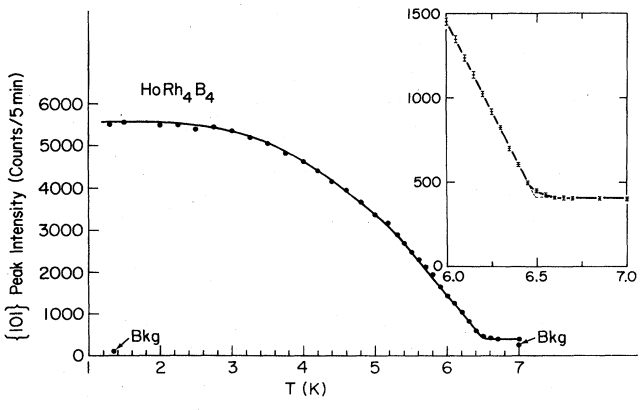

FIG. 3. Observed peak intensity, which is a measure of the square of the magnetization, as a function of temperature for $HoRh_4B_4$. The inset shows that there is very little critical scattering associated with this phase transition. The linear dependence of I vs T in the vicinity of T_c (6.47 K) reveals the mean-field behavior of this transition, and the solid curve is mean-field theory for $S=\frac{1}{2}$ (see Ref. 17).

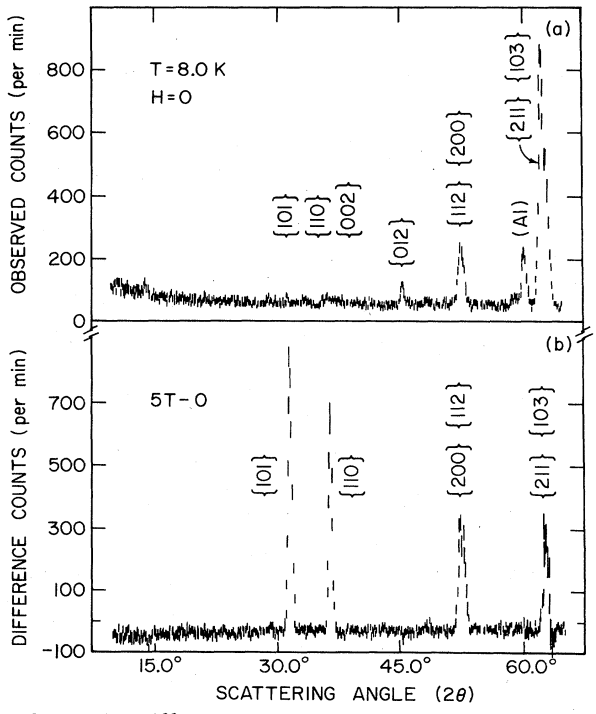

FIG. 4. (a) Diffraction data above the magnetic phase transition in zero applied field. The observed peaks are nuclear in origin. (b) Induced-moment diffraction data, obtained by subtracting the zero-field data from the data measured in an applied magnetic field of 5 T.

no spontaneously aligned magnetic moment, but a moment can be induced by applying a magnetic field. Diffraction data are shown in Fig. 4 for a temperature of 8.0 K. In zero field only the nuclear peaks are evident as shown in Fig. 4(a). Subtracting these data from the scattering with 5 T applied yields the data shown in Fig. 4(b). It is quite evident that the intensities of the magnetic peaks are much stronger than the nuclear intensities, as is the case in the ordered magnetic state. For reflections such as {102} and {201} we see that there is no magnetic intensity, as expected, since $F_M = 0$. We also remark that the intensities of the magnetic-impurity peaks (I) depend on H. Measurements of the temperature dependence of these intensities (in zero field) show that this magnetic transition occurs at ~ 19 K.

Figure 5(a) shows in detail that once again there is no discernible magnetic contribution to {00l}-type reflections so that the magnetization is indeed highly anisotropic as inferred from bulk magnetization measurements.[26] Thus, the magnetic field cannot induce an appreciable magnetic moment perpendicular to the c axis for fields up to 7 T, within the experimental sensitivity of $0.4\mu_B$. The field dependence of the {101} peak is shown in the bottom half of Fig. 5, where we see that 7 T is sufficient to nearly saturate the intensity of this reflection. The value of the induced moment is close to the value observed in the ordered state at low temperature. We remark that the present technique has two advantages over conventional magnetization measurements in powders. Firstly, information about the magnetic anisotropy can be obtained (in systems with symmetry lower than cubic) both in the ordered as well as the paramagnetic state on powdered specimens. In the fortunate case where the easy magnetic axis coincides with a unique crystallographic axis the magnetic structure in fact can be solved completely. Secondly, the neutrons can distinguish between the magnetic properties of the phase of interest and any possible magnetic impurities which might be present since the Bragg peaks generally will occur at different scattering angles. Thus, the measurements are usually easier to interpret. A quantitative analysis of our field-dependent data will be presented elsewhere.[11]

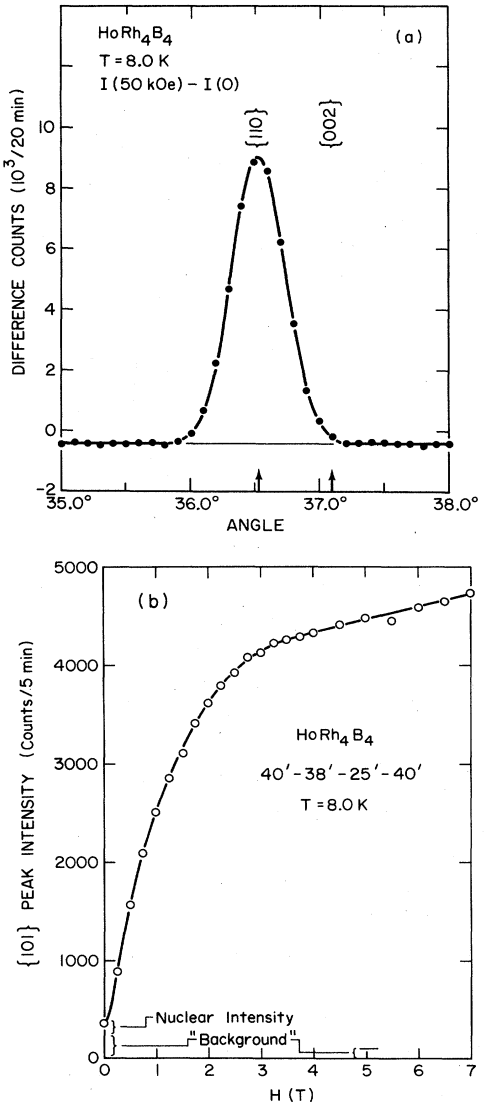

FIG. 5. (a) The {110} and {002} magnetic peaks observed in an applied field of 5 T. The absence of intensity at the {00l}-type positions directly reveals the Ising-like magnetic character of this system. (b) Observed intensity of the {101} peak as a function of H at 8.0 K.

B. $(Er_{1-x}Ho_x)Rh_4B_4$

In this alloy series superconductivity appears for concentrations below the "multicritical" point of $x_c \sim 0.9$. Figure 6 shows the bulk susceptibility and magnetization

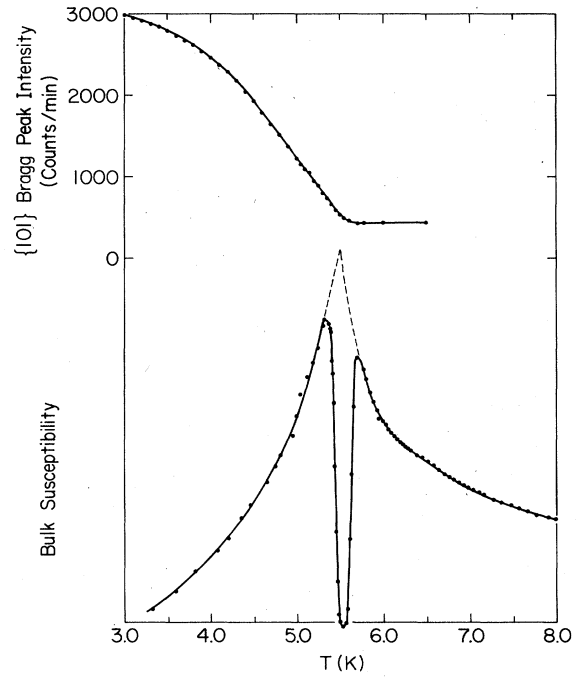

FIG. 6. Observed bulk susceptibility and neutron Bragg-peak intensity for $(Er_{0.11}Ho_{0.89})Rh_4B_4$. The neutron data reveal a transition to long-range ferromagnetic order at 5.56 K, which is in good agreement with the magnetic transition temperature obtained from the bulk susceptibility data extrapolated into the superconducting region (dashed curve).

data on a sample of $x=0.89$, which is slightly rich in Er such that the system is superconducting over a small temperature interval. The susceptibility shows the customary λ-type anomaly indicative of a ferromagnetic transition (for an Ising system), except that in the vicinity of T_M the sample becomes superconducting. The magnetic phase transition itself is masked in the bulk susceptibility measurements by the diamagnetic response of the superconducting screening currents. The neutrons, on the other hand, directly probe the atomic ($4f$) magnetization through the magnetic contribution to the Bragg reflections and reveal the transition to long-range magnetic order. The data show that the intensity is linear in the vicinity of T_M, indicative of the mean-field behavior of the holmium system. This linearity allows an accurate determination of $T_M=5.56$ K. This transition temperature agrees very well with the T_M deduced from the susceptibility measurements when they are extrapolated into the superconducting region. One noteworthy point is that in this particular sample the bulk susceptibility has a *minimum* at T_M, due to the superconductivity, rather than a maximum. The results of Fig. 6 emphasize the complementary nature of these two experimental techniques.

Figure 7 shows the scattering at relatively small wave vectors for this material, taken with a triple-axis spectrometer. In more conventional systems a strong peak as a function of temperature will be evident in data of this type, but the weak critical scattering produces no such peak in the wave-vector-dependent susceptibility $\chi(Q)$ for this system for this range of Q. This is a further indication of the mean-field behavior of this material. We will discuss this behavior in more detail when we present our small-angle scattering data for the $x=0.84$ compound.

The Bragg-peak intensity and small-angle data show no influence from the superconductivity, either in terms of a reduction in the expected magnetization or in terms of any hysteresis in the magnetization or susceptibility. The data in fact suggest that magnetic order may coexist with superconductivity over a limited interval of temperature, and can be interpreted with the assumption that an internal magnetization develops in the superconducting state, with the superconductivity being quenched when the internal field becomes sufficiently large. The temperature interval where the coexistence appears to occur, however, is quite small for this alloy.

At a lower holmium concentration of $x=0.84$ the temperature interval of superconductivity is larger as shown in Fig. 8. The top part of the figure shows the measured resistivity, and the bottom portion the ac susceptibility. The superconducting transition temperatures derived from these data are $T_{c1}=5.95$ K, and $T_{c2}=4.95$ K. The $\{101\}$ Bragg-peak intensity, on the other hand, reveals a magnetic transition temperature of 5.30 K as shown in Fig. 9. The magnetic intensity is still linear in the vicinity of T_M, demonstrating the persistence of mean-field behavior at this lower concentration. We have observed no evidence for a reduction in the magnetization in the region where superconductivity is present, nor have we observed any thermal-cycling effects either above or below T_{c2}, in contrast to the behavior clearly observed for $x=0.6$.[17] Again our data are consistent with the assumption that an internal magnetization develops in the superconducting phase, and increases in amplitude to the point where the superconductivity is quenched.

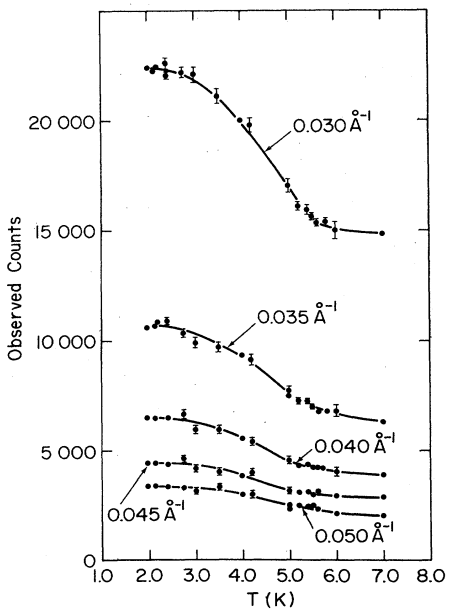

FIG. 7. Small-angle neutron-scattering data taken with a conventional triple-axis spectrometer for $(Er_{0.11}Ho_{0.89})Rh_4B_4$. The critical fluctuations in the system are quite weak, producing no observable peak in the wave-vector-dependent susceptibility $\chi(Q)$.

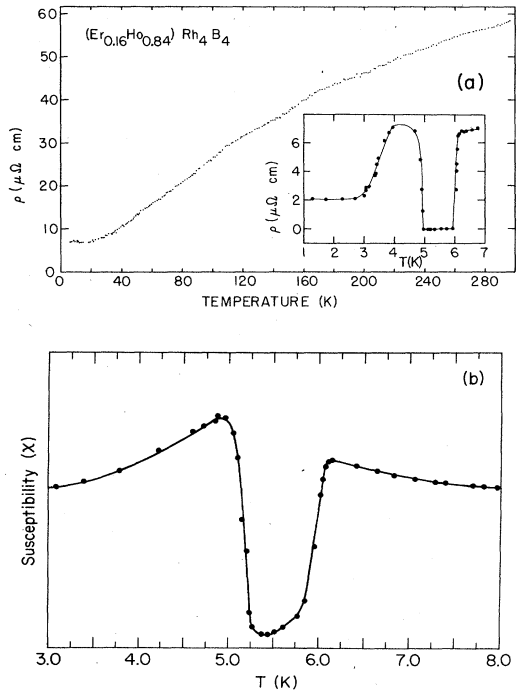

FIG. 8. (a) Resistivity and (b) bulk susceptibility for $x=0.84$. The onset of superconductivity occurs at $T_{c1}=5.95$ K with a reentrant transition at 4.95 K.

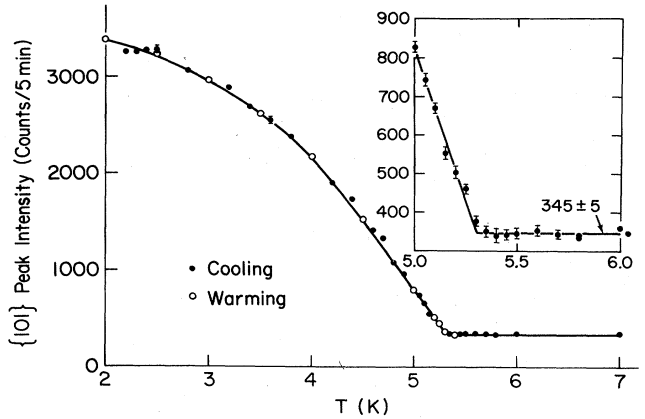

FIG. 9. The {101} Bragg-peak intensity for $(Er_{0.16}Ho_{0.84})Rh_4B_4$. The transition to long-range magnetic order occurs at 5.30 K, well inside the superconducting interval of $0.495 < T < 0.595$ K. The magnetic order appears to be ferromagnetic in nature within our experimental resolution of 0.003 $Å^{-1}$.

An interesting question in this system is whether there is an oscillatory magnetization such as has been observed in the related systems $HoMo_6S_8$ and $HoMo_6Se_8$ (and $ErRh_4B_4$). One possible interpretation of the above results, for example, would be that the long-range magnetic order is oscillatory in nature, but with a wavelength λ which is too long to be resolved with conventional diffraction (i.e., $\lambda \gtrsim 300$ Å). Figure 10 shows some neutron data taken with the small-angle neutron-scattering (SANS) instrument at NBS. A neutron wavelength of 6.25 Å was employed in the "high-resolution" mode.[23] The total intensity measured on the two-dimensional position-sensitive detector shows a very sharply defined phase transition at (5.32±0.02) K, while the expanded scale reveals that there are indeed weak critical fluctuations associated with the transition. The sharp character of the transition as evidenced in these data precludes the possibility of any significant inhomogeneities in these samples. We also did not observe any thermal hysteresis in the intensities.

The magnetic intensity as a function of the magnitude of the wave vector Q is shown in Fig. 11 for several temperatures. These data have been obtained by subtracting the scattering at high temperature (10 K) from the intensity observed at the temperature indicated, and are directly related to the wave-vector-dependent susceptibility $\chi(Q)$ since the inelasticity of the (critical) scattering should be

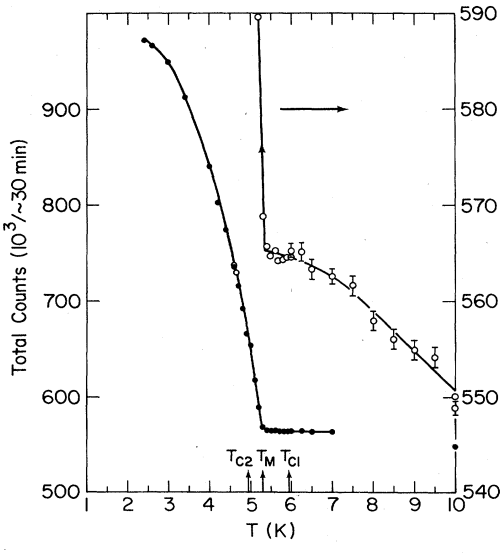

FIG. 10. Total intensity of the two-dimensional position-sensitive detector as a function of temperature, showing the sharp onset of scattering at T_M for $(Er_{0.16}Ho_{0.84})Rh_4B_4$. The expanded scale shows that there is a weak critical component to the scattering as well.

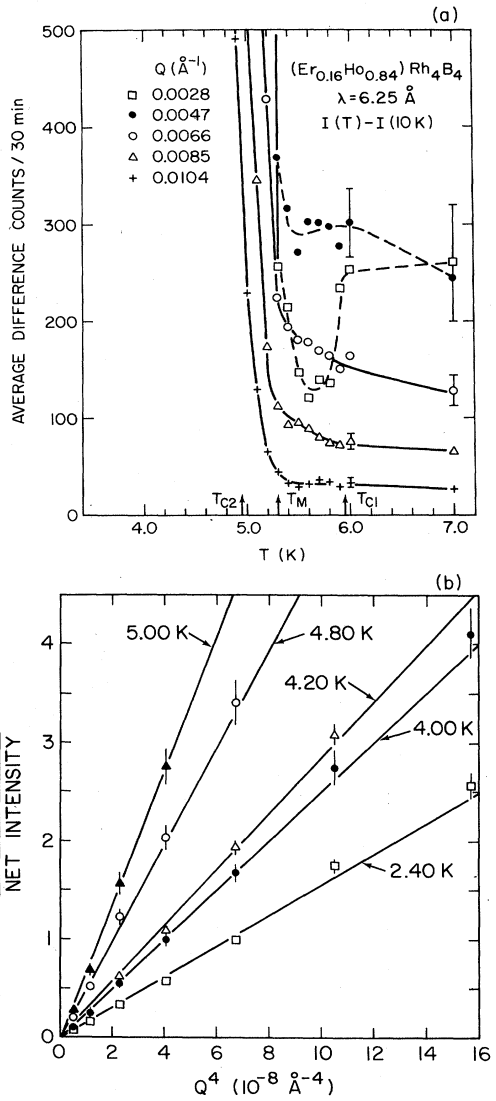

FIG. 11. (a) Intensity of the small-angle scattering at several wave vectors Q above the magnetic phase transition T_M. Note that there is an indication that the scattering at the smallest wave vectors is reduced below T_{c1}. (b) Inverse intensity as a function of Q^4 below T_M. The linear behavior indicates that the scattering originates from variations in the magnetization density in real space which are very large compared to $1/Q$.

small compared to the incident neutron energy. The top portion of the figure indicates that above the magnetic phase transition the critical scattering is quite weak and the range of the magnetic correlations is short. We remark that in the superconducting state the susceptibility $\chi(Q)$ may be modified due to screening of the magnetic fluctuations by the supercurrents.[27] Such screening should become important for length scales of the order of or larger than the London penetration depth λ_L (typically $\sim 10^3$ Å) so that the effects of superconductivity on the paramagnetic fluctuations should be evident for $Q \lesssim 1/\lambda_L$. For the present system λ_L is not known, but we note that the intensity at the smallest wave vectors does in fact decrease below T_{c1} rather than increase in intensity as expected when approaching the transition. This is an important observation because it would be a direct confirmation of the theoretical foundations on which most theories of these systems are based. The statistical uncertainties in the present case are quite large, however, due to the strong metallurgical scattering from these powdered specimens. It is also at the small-Q limit of the spectrometer. Consequently these results can be taken only as suggestive at present, not definitive.

The data below T_M are shown in the lower half of Fig. 11. We see that the scattering is in good agreement with the assumption that the intensity obeys a relation of the Porod form[28]

$$S(Q)=\frac{A(T)}{Q^4}\ , \tag{8}$$

where $A(T)$ is a temperature-dependent amplitude. This general dependence on Q is customary for scattering from objects whose spatial extent is much larger than the inverse wave-vector range of interest.[28,29] Thus, the most likely interpretation of our data below T_M is that the scattering originates from domains (or domain walls) whose average size is much larger than $1/Q \sim 250$ Å. Another possibility, however, is that the system has developed an oscillatory magnetic state, but with a wavelength which is out of the range of our observations. We remark that there is no evidence for an oscillatory component within the accessible range of Q, and there is no evidence for any thermal-hysteresis effects such as have been observed in some related systems.[5,7–10]

The lowest concentration sample we have studied is $x=0.75$, where we observed a T_{c1} of 6.3 K and a reentrant transition of 4.1 K. The {101} Bragg-peak intensity is shown in Fig. 12. Below T_{c2} there is a temperature interval where the intensity is linear as observed at larger x, and extrapolating these data to higher temperatures (dashed line) yields an expected magnetic transition temperature of ~ 4.75 K. In the superconducting region, however, there is a clear reduction in the intensity as well as an apparent rounding similar to the "smearing" observed in $ErRh_4B_4$. This "smearing" makes it more difficult to pinpoint the actual transition temperature, but it is certainly between 4.6 and 4.7 K. Thus, the observed T_M is well above T_{c2} in this case. We also remark that we have observed no thermal-cycling effects; the data are completely reproducible on warming and cooling. A similar reduction in the magnetization has been observed[17] at

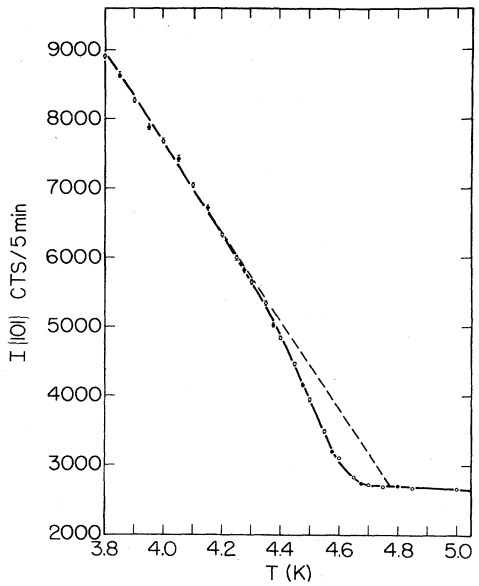

FIG. 12. Temperature dependence of the {101} Bragg peak for $x=0.75$, showing a clear anomaly in the magnetization in the region where superconductivity exists. However, no hysteresis in the magnetization or susceptibility is observed.

$x=0.6$, but the magnetic transition appeared sharper in that case, with T_M coinciding with a spike in the heat capacity suggesting that $T_M=T_{c2}$. In addition, thermal-cycling effects were observed in that case, but only below T_{c2}.

IV. DISCUSSION

A. Mean-field behavior of $HoRh_4B_4$

Our field-dependent measurements demonstrate that the holmium moments are locked along the (unique) tetragonal axis so that the magnetic properties at low temperatures should be well described by an Ising Hamiltonian in three spatial dimensions ($d=3$). For the usual case of short-range exchange interactions, the upper marginal dimensionality d^*, above which the mean-field description of the critical phenomena is valid, is four. Consequently we might expect conventional critical behavior with nonclassical exponents.[30] In the low-temperature ferromagnets of present interest, however, dipolar interactions undoubtedly will be important, and the presence of such long-range interactions can qualitatively change the nature of the transition.[31,32] In particular for an Ising ferromagnetic with dipole interactions only the upper-marginal dimensionality is reduced to $d^*=3$, in which case we expect only logarithmic corrections to the mean-field results. We remark at the outset of this discussion that it will be difficult to make any detailed comparisons of our data with theory since we obtain only crystallographically averaged data on these powders. Rather, we adopt the more modest goal of discussing the possible origin of the mean-field-like behavior which has been observed in this system. To this end we will briefly review the theoretical expectations for Ising dipolar ferromag-

nets,[30–32] and then compare the observed behavior with the experimental data on related systems such as $LiTbF_4$ where detailed observations of the critical phenomena have been made on single-crystal specimens.[33–37]

At the marginal dimensionality $d=d^*$ calculations of critical phenomena can be carried out very accurately since they do not have to rely on techniques such as ϵ or $1/n$ expansions. For a dipolar-coupled Ising ferromagnet the critical behavior should be given by the mean-field predictions multiplied by logarithmic factors.[31,32] For example, the magnetization is expected to follow

$$M=Bt^{1/2}|\ln t|^{1/3} \tag{9}$$

(with B a critical amplitude) rather than the more customary power-law behavior given by Eq. (6) (with $\beta=\frac{1}{2}$). In the more general case where both dipolar and exchange contributions must be considered, we expect a crossover from three-dimensional Ising to dipolar behavior as the critical temperature is approached. This crossover occurs when[32]

$$t^{\phi}\simeq\hat{g}=\frac{(g\mu_B)^2}{Ja^d}\ , \tag{10}$$

where $g\mu_B$ is the magnetic moment per spin, a is the (cubic) lattice parameter, J is the (isotropic) exchange constant, and ϕ is the crossover exponent. This crossover in characteristic behavior will occur for all ferromagnets sufficiently close to the transition, but the dipolar effects play a much more important role in materials where the exchange coupling is weak.

These theoretical ideas have been tested in detail for a number of materials. In $LiTbF_4$, for example, the (antiferromagnetic) exchange interactions are only 25% of the dipolar contributions[34] ($\mu_z=8.9\mu_B$), leading to a ferromagnetic phase transition with $T_c=2.87$ K. Of particular relevance to the present discussion are the following points. The first is that the neutron-scattering measurements[33,34] determined a critical exponent $\beta=0.45$, close to the mean-field value. Indeed the presence of the logarithmic correction terms could only be determined with very precise measurements.[35–37] Secondly, the critical fluctuations were found to be very weak in amplitude (and highly anisotropic).[33]

To estimate the ratio of dipolar-to-exchange energies for $HoRh_4B_4$, we first calculate the dipole energy. For two spins a distance r apart, the energy of interaction is

$$E=0.6229\mu_z^2\frac{(1-3z^2/r^2)}{r^3}\ , \tag{11}$$

where z is the distance along the Ising axis. The numerical constant has been chosen such that if μ_z is in Bohr magnetons, z and r in angstroms, then E is in degrees Kelvin. For nearest-neighbor moments in $HoRh_4B_4$ we have $E=-0.002\,05\mu_z^2=-0.205$ K, assuming that each moment is $10\mu_B$. (For $LiTbF_4$ we have $E=-0.533$ K.) To calculate the total magnetic contribution for any particular spin we sum Eq. (11) over all other spins in the system, which yields $E=-0.859$ K. The dipole energy needed to reverse a spin is then twice this value. Clearly the dipolar effects will be quite important in this material although the dipole energy alone is certainly not sufficient to explain the observed transition temperature of 6.5 K. We thus assume that the additional ferromagnetic energy needed is of exchange origin. From mean-field theory we obtain the estimate $J=3T_M^{(ex)}/[\delta S(S+1)]=1.59$ K, where $S=\frac{1}{2}$ and $\delta=12$ is the (approximate) number of nearest neighbors. Finally, from Eq. (10) we can then estimate the dipolar crossover $\hat{g}$ as 2.4. We therefore conclude that the observed mean-field behavior, at least in the critical region, originates from the dipolar interactions in $HoRh_4B_4$. The same estimate for $LiTbF_4$ gives $\hat{g}\sim 16$ so that dipolar effects completely dominate in this "ideal" dipolar material. For an exchange-dominated system like iron, on the other hand, we have $\hat{g}\sim 0.002$.

Note that we need to assume a ferromagnetic exchange interaction for $HoRh_4B_4$ in order to explain the observed transition temperature, whereas in $LiTbF_4$ the (measured) exchange is negative. The importance of the exchange interaction in determining T_M is exemplified by the results for $Ho(Rh_{1-x}Ir_x)_4B_4$, where T_M is found to decrease rapidly with increasing x and the magnetic structure becomes antiferromagnetic[38] for sufficiently large x. The dipolar interactions for this alloy of course should be independent of x if we assume that the crystal-field ground state is not disturbed by the randomness introduced on the Rh sublattice.

One final comment concerns the observed mean-field behavior for the magnetization of $HoRh_4B_4$ over the full temperature range as shown in Fig. 3 (and Ref. 17). In $LiTbF_4$ the comparison is less satisfactory, which opens the question of the range and nature of the nondipolar interactions in these magnetic superconductors. In the composition region below x_c the magnetic-superconducting coupling may be quite long in range as the system tries to order, since both the exchange as well as the electromagnetic interactions are coupled, and the length scales for the superconducting state (the London penetration depth and the coherence length ξ) are large. Indeed, for the superconducting transition itself the natural length scales involved lead to mean-field behavior for properties such as the specific heat. Of course for $x>x_c$ the superconducting state is suppressed, but the propensity to be a superconductor is still present and it may be necessary to incorporate these energetics (and electronic length scales) to obtain a full understanding of these systems. Precise measurements on single-crystal specimens will be needed to unravel the details of these various interactions.

B. $x<x_c$

A summary of the transition temperatures and ordered magnetic moments for our samples is given in Table I. When the magnetic order develops, we see that there is a region of temperature where superconductivity is maintained for $x<x_c$, with the interval of coexistence increasing with decreasing x. In comparing the transition temperatures measured with neutrons and bulk measurements, it is clearly essential to take the data on identical samples. It is also essential to establish the accuracy of the temperature scales for the two measurements in order

TABLE I. Measured transition temperatures for the various alloys investigated. The low-temperature magnetic moment is calculated per Ho ion, while the average moment at T_{c2} is calculated per formula unit so that it is directly related to the magnetization density.

x	T_{c1} (K)	T_{c2} (K)	T_M (K)	$\mu(T=0)$ (μ_B)	$\bar{\mu}(T=T_{c2})$ (μ_B)
1.0			6.47	8.58	
0.89	5.71	5.33	5.56	8.76	2.2
0.84	5.95	4.95	5.33	7.6	2.5
0.75	6.44	4.07	4.75	8.3	3.4

to effect a reliable comparison. For the pure holmium compound we found that the magnetic transition determined from susceptibility agreed with the neutron measurements within the combined experimental errors of ~ 0.03 K. In addition, the helium bath provides an international standard for thermometry in this temperature range. Consequently, we believe our temperature measurements should be accurate on an absolute scale to about ± 0.02 K over the entire temperature range of interest. The measured differences between the reentrant superconducting transitions and the magnetic transition temperatures, on the other hand, are as large as 0.68 K. Thus, it is impossible to attribute these large differences in transition temperatures to discrepancies in thermometry.

Theoretically, coexistence of pure ferromagnetism and superconducting is not expected to be possible so that we expect any ordered magnetic state to be nonuniform on some length scale.[27] In the three related compounds $ErRh_4B_4$, $HoMo_6S_8$, and $HoMo_6Se_8$, a sinusoidal magnetic state in fact is found to coexist with superconductivity with a characteristic wavelength λ_M of the magnetic order parameter of $\sim 10^2$ Å. In the present alloy one possible explanation for our experimental results is that λ_M is considerably larger than 10^2 Å, and hence is outside our experimental range. We can make an estimate of q_c for the present system by assuming that the magnetic stiffness parameter $\gamma \propto T_M$ and the (zero-temperature) London penetration depth $\lambda_L^{(0)} \propto 1/T_{c1}$. Then the theoretical relation[39,40] suggests that

$$q_c \propto (\gamma \lambda_L)^{-1/2} \propto \left[\frac{T_{c1}}{T_M}\right]^{1/2} . \tag{12}$$

For the sake of this estimate we choose to use the measured parameters for $HoMo_6S_8$ since this material has a (similar) saturated magnetic moment of $\mu_z(0)=9\ \mu_B$, and it has the unique crystallographic axis as the preferred magnetic direction; we have $T_{c1}=1.8$ K, $T_M=0.7$ K, and $q_c=0.03$ Å^{-1}. Scaling these values via Eq. (12) then yields for $x \sim x_c$ a $q_c \sim 0.005$ Å^{-1} at low temperatures, which is just in the range of accessible wave vectors. However, near T_{c1} λ_L should be strongly temperature dependent, with $1/\lambda_L \to 0$ as $T \to T_{c2}$. Thus, we would expect the actual q_c to be considerably smaller than this estimate, and hence out of the range of our experimental limit of ~ 0.003 Å^{-1}. An alternate possibility is that a vortex lattice has formed spontaneously in the superconductivity region, with a periodicity which is again beyond the present limits of measurements. Clearly data at smaller q could be illuminating. We remark that these oscillatory magnetic states are considerably shorter in wavelength, and physically are fundamentally different, than the typical formation of periodic domain walls.[41]

Finally we compare our results with those at lower holmium concentrations, where a distinct peak in the specific heat has been observed at T_M. As we approach x_c the anomaly in T_M and the spike in C_v become smaller, and they may rapidly reduce in size when $T_M(x) \to T_{c1}(x)$ and $x \to x_c$. This region in (x, T) is characterized by a strong variation in λ_L, which may alter the balance of energies near x_c and produce different physical behavior, particularly with regard to possible modulated magnetic states. For example, as $x \to x_c$ conventional ferromagnetic domains (where the domain walls are possibly superconducting[42]) and the sinumagnetic-superconducting states may not be distinct. Present samples and experimental techniques are not adequate to address these questions at the moment, but they should prove to be interesting areas of endeavor in the future.

ACKNOWLEDGMENTS

We would like to thank W. B. Daniels, B. D. Dunlap, R. A. Ferrell, W. C. Koehler, S. M. Lambert, M. B. Maple, H. A. Mook, R. M. Moon, and O. A. Pringle for helpful discussions and assistance. The research at Maryland was supported by the U. S. National Science Foundation, Grant No. DMR 83-19936. Ames Laboratory is operated for the U. S. Department of Energy by Iowa State University under Contract No. W 7405-Eng-82. Research at Ames was supported by the Director for Energy Research, Office of Basic Sciences, Grant No. WPAS-KC-02-02-02.

*Permanent address.
†Permanent address: Department of Physics, National Taiwan Normal University, Taipei, Taiwan, Republic of China.

[1]For a recent review of these materials, see *Topics in Current Physics*, edited by Ø. Fischer and M. B. Maple (Springer-Verlag, New York, 1983), Vols. 32 and 34.
[2]W. A. Fertig, D. C. Johnston, L. E. DeLong, R. W. McCallum, M. B. Maple, and B. T. Matthias, Phys. Rev. Lett. **38**, 987 (1977).
[3]D. E. Moncton, D. B. McWhan, J. Eckert, G. Shirane, and W. Thomlinson, Phys. Rev. Lett. **39**, 1164 (1977).
[4]M. Ishikawa and Ø. Fischer, Solid State Commun. **23**, 37 (1977).
[5]J. W. Lynn, D. E. Moncton, W. Thomlinson, G. Shirane, and R. N. Shelton, Solid State Commun. **26**, 492 (1978).
[6]J. W. Lynn, J. A. Gotaas, R. W. Erwin, R. A. Ferrell, J. K. Bhattacharjee, R. N. Shelton, and P. Klavins, Phys. Rev. Lett. **52**, 133 (1984).
[7]D. E. Moncton, D. B. McWhan, P. H. Schmidt, G. Shirane, W. Thomlinson, M. B. Maple, H. B. MacKay, L. D. Woolf, Z.

Fisk, and D. C. Johnston, Phys. Rev. Lett. **45**, 2060 (1980).
[8]S. K. Sinha, G. W. Crabtree, D. G. Hinks, and H. A. Mook, Phys. Rev. Lett. **48**, 950 (1982).
[9]J. W. Lynn, G. Shirane, W. Thomlinson, and R. N. Shelton, Phys. Rev. Lett. **46**, 368 (1981); Phys. Rev. B **24**, 3817 (1981).
[10]J. W. Lynn, J. L. Ragazzoni, R. Pynn, and J. Joffrin, J. Phys. (Paris) Lett. **42**, L45 (1981); J. W. Lynn, R. Pynn, J. Joffrin, J. L. Ragazzoni, and R. N. Shelton, Phys. Rev. B **27**, 581 (1983).
[11]B. D. Dunlap, L. N. Hall, F. Behroozi, G. W. Crabtree, and D. G. Niarchos, Phys. Rev. B **29**, 6244 (1984); B. D. Dunlap and J. W. Lynn (unpublished).
[12]G. W. Crabtree, F. Behroozi, S. A. Campbell, and D. G. Hinks, Phys. Rev. Lett. **49**, 1342 (1982).
[13]D C. Johnston, W. A. Fertig, M. B. Maple, and B. T. Matthias, Solid State Commun. **26**, 141 (1978).
[14]H. B. MacKay, L. D. Woolf, M. B. Maple, and D. C. Johnston, Phys. Rev. Lett. **42**, 918 (1979); **43**, 89(E) (1979).
[15]J. W. Lynn, in *Ternary Superconductors,* edited by G. K. Shenoy, B. D. Dunlap, and F. Y. Fradin (North-Holland, New York 1981), p 51; J. W. Lynn, J. Less-Common Met. **94**, 75 (1983).
[16]J. W. Lynn, R. N. Shelton, H. E. Horng, and C. J. Glinka, Physica (Utrecht) **120B**, 224 (1983).
[17]H. A. Mook, W. C. Koehler, M. B. Maple, Z. Fisk, D. C. Johnston, and L. D. Woolf, Phys. Rev. B **25**, 372 (1982).
[18]H. R. Ott, G. Keller, W. Odoni, L. D. Woolf, M. B. Maple, D. C. Johnston, and H. A. Mook, Phys. Rev. B **25**, 477 (1982).
[19]G. H. Lander, S. K. Sinha, and F. Y. Fradin, J. Appl. Phys. **50**, 1990 (1979).
[20]R. N. Shelton, C. U. Segre, and D. C. Johnston, Solid State Commun. **33**, 843 (1980).
[21]J. M. Vandenberg and B. T. Matthias, Proc. Nat. Acad. Sci. U. S. A. **74**, 1336 (1977).
[22]G. E. Bacon, *Neutron Diffraction* (Oxford, Bristol, 1975), 3rd edition, p. 111, Chap. 6.
[23]C. J. Glinka, in *Neutron Scattering—1981,* edited by John Farber, Jr. (AIP, New York, 1981), p. 395.
[24]H. Adrian, K. Müller, and G. Saemann-Ischenko, Phys. Rev. B **22**, 4424 (1980).
[25]M. Blume, A. J. Freeman, and R. E. Watson, J. Chem. Phys. **37**, 1245 (1962); **41**, 1878 (1964).
[26]H. C. Ku, F. Acker, and B. T. Matthias, Phys. Lett. **76A**, 399 (1980).
[27]For a recent review of the theory see P. Fulde and J. Keller, in *Topics in Current Physics,* Ref. 1, Chap. 12.
[28]G. Porod, Kolloid Z. **124**, 83 (1951); **125**, 51 (1952).
[29]P. Debye, H. R. Anderson, and H. Brumberger, J. Appl. Phys. **28**, 679 (1957).
[30]For a review, see K. G. Wilson and J. Kogut, Phys. Rep. **12C**, 75 (1974).
[31]A. I. Larkin and D. E. Khmel'nitskii, Zh. Eksp. Teor. Fiz. **56**, 2087 (1969) [Sov. Phys.—JETP **29**, 1123 (1969)].
[32]A. Aharony and M. E. Fisher, Phys. Rev. B **8**, 3323 (1973); A. Aharony, *ibid.* **8**, 3363 (1973).
[33]J. Als-Nielsen, L. M. Holmes, and H. J. Guggenheim, Phys. Rev. Lett. **32**, 610 (1974); J. Als-Nielsen, *ibid.* **37**, 1161 (1976).
[34]L. M. Holmes, J. Als-Nielsen, and H. J. Guggenheim, Phys. Rev. B **12**, 180 (1975); J. Als-Nielsen, L. M. Holmes, F. K. Larsen, and H. J. Guggenheim, *ibid.* **12**, 191 (1975).
[35]G. Ahlers, A. Kornblit, and H. J. Guggenheim, Phys. Rev. Lett. **34**, 1227 (1975).
[36]J. A. Griffin and J. D. Litster, Phys. Rev. B **19**, 3676 (1979).
[37]R. Frowein, J. Kötzler, B. Schaub, and H. G. Schuster, Phys. Rev. B **25**, 4905 (1982).
[38]H. C. Hamaker, H. C. Ku, M. B. Maple, and H. A. Mook, Solid State Commun. **43**, 455 (1982).
[39]E. I. Blount and C. M. Varma, Phys. Rev. Lett. **42**, 1079 (1979); H. S. Greenside, E. I. Blount, and C. M. Varma, *ibid* **46**, 49 (1981).
[40]R. A. Ferrell, J. K. Bhattacharjee, and A. Bagchi, Phys. Rev. Lett. **43**, 154 (1979).
[41]T. Garel and S. Doniach, Phys. Rev. B **26**, 325 (1982).
[42]M. Tachiki, A. Kontani, H. Matsumoto, and H. Umezawa, Solid State Commun. **32**, 599 (1979).